



An experimental investigation of dam-break induced flood waves for different density fluids

Hatice Ozmen-Cagatay^{a,*}, Evren Turhan^b, Selahattin Kocaman^c

^a Department of Civil Engineering, Cukurova University, 01330, Adana, Turkey

^b Department of Civil Engineering, Adana Alparslan Turkes Science and Technology University, 01180, Adana, Turkey

^c Department of Civil Engineering, Iskenderun Technical University, 31200, Hatay, Turkey

ARTICLE INFO

Keywords:

Dam-break experiment
Image processing
CFD
RANS
Different density fluids

ABSTRACT

The present study aims to investigate the effect of various fluids on dam-break flow propagation in a rectangular and horizontal channel under dry bed conditions. Laboratory experiments were carried out to produce dam-break flood waves in a tank by the sudden release of a movable gate that divided the tank into a reservoir and a downstream channel. In these experiments, three different fluids were used as Newtonian fluids in the reservoir: normal water, sunflower oil, and salt water. A digital image processing technique was adopted for the experimental characterization of the dam-break waves. Instantaneous free surface profiles of the dam-break flow were captured by a high-speed camera. Free-surface profiles for different times and time evolution of the flow depths at four selected locations were determined. The types of fluids had an effect on the results due to their specific characteristics such as density and viscosity. Furthermore, numerical simulation of the problem was performed by Reynolds-averaged Navier-Stokes (RANS) and Volume of Fluid (VOF) based software Flow-3D. When the experimental data were compared with the numerical simulation results, there was good agreement for the elapsed time and selected measuring locations.

1. Introduction

Dam-break induced catastrophic flood waves may act as a tsunami. Although a dam-break wave may not simulate actual tsunami conditions exactly, they have been successfully used by researchers in their studies on tsunami inundations and the design of sea dikes for protecting on-shore structures (Prabu et al., 2019), because, dam break waves have several hydrodynamic similarities to tsunami waves (Chanson et al., 2003). Dam-break flow is a complex fluid dynamics problem due to its nonlinear and rapidly varied unsteady flow characteristics. There is always a risk that dam-breaks can be caused by overtopping and catastrophic rainfalls, which can cause catastrophic damages (Ozmen-Cagatay and Kocaman, 2010; Tayfur and Guney, 2013; Zhang, and Tan, 2014; Li and Yu, 2019; Issakhov and Imanberdiyeva, 2019). Description of the chaotic flow behavior is very important in terms of taking emergency plans. For many years, hydraulic researchers have examined challenging dam-break flow estimations with analytical, numerical and experimental methods. In the past, analytical solutions to dam-break flow were obtained under idealized conditions. Stoker (1957) extended Ritter's (1892) dry bed solution to a wet bed case by

solving the Saint-Venant equations using the method of characteristics and relevant shock-wave solutions. With recent development in computer technology, many numerical models have been developed for the dam-break problems by solving the shallow water equations (SWE) and Reynolds-averaged Navier Stokes equations (RANS) (Shigematsu, 2004; Marsooli and Wu, 2014; Kamra et al., 2018; Yang et al., 2018; Kesserwani et al., 2019; Prabu et al., 2019; Cantero-Chinchilla et al., 2019). VOF-based CFD models that allow SWE and RANS solutions have also been adopted to simulate dam-break flow (Ozmen-Cagatay and Kocaman, 2011; Oertel and Bung, 2012; Ozmen-Cagatay et al., 2014; Kocaman and Ozmen-Cagatay, 2015; Hu and Zhang, 2018; Turhan et al., 2018; Khoshkonesh et al., 2019; Yang et al., 2019; Wang et al., 2020; Issakhov and Borsikbayeva, 2021). With Direct Numerical Simulation (DNS), all scales of wave motion of a turbulent flow like a dam-break example can be calculated. For these turbulent flows, the DNS involves a large number of grid modes. RANS models can assist describing the boundary layer while restraining solution process time to sensible limits (Wilcox, 2000; Ozgokmen et al., 2007). In this research, the numerical analysis was conducted with the VOF-based industrial CFD program Flow-3D, adopted previously in numerous studies (Biscarini,

* Corresponding author.

E-mail addresses: hatmen@cu.edu.tr (H. Ozmen-Cagatay), eturhan@atu.edu.tr (E. Turhan), selahattin.kocaman@iste.edu.tr (S. Kocaman).

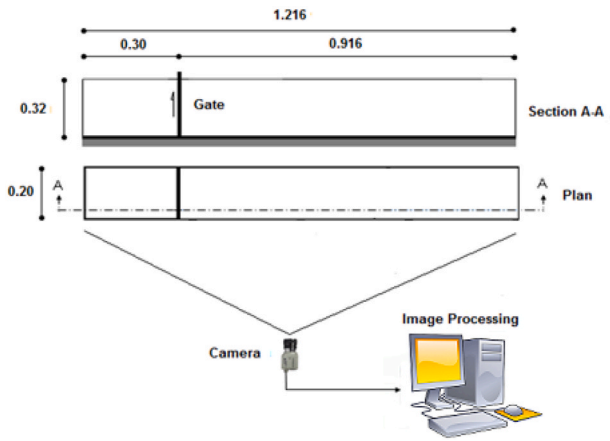


Fig. 1. Experimental set-up with lengths in meters (Turhan et al., 2018).

2010; Ozmen-Cagatay and Kocaman, 2011; Oertel and Bung, 2012; Khrabry et al., 2016; Hu et al., 2018; Yang et al., 2019). Over the last decade, the Level Set (LS) method has become popular for simulating gas-liquid two-phase flows because of its advantages (Ningegowda and Premachandran, 2014; Balcazar et al., 2016; Gu et al., 2018; Li and Yu, 2019). VOF and LS solver are well-known methods in solid-fluid interface problems. Yu et al. (2019) developed a Coupled Level Set, VOF and Immersed Boundary (CLSVOF/IB) method, and applied it to simulating the interaction between dam-break flow and stationary obstacles. As an alternative to the CFD models, mesh-free modeling with Smoothed-Particle Hydrodynamics (SPH) method was used in dam-break flow simulations (Turhan, 2017; Turhan et al., 2019a,b; Soleimani and Ketabdari, 2020).

While the numerical models enable the simulation of complex dam-break flows, validation with field data is necessary. However, limited field data are available; thus, laboratory experiments are used alternatively. Previous experimental works have investigated the initial stages of the dam-break flow (Bellos et al., 1992; Lauber and Hager, 1998; Stansby et al., 1998; Janosi et al., 2001; Bukreev and Gusev, 2005; Eaket et al., 2005; Ozmen-Cagatay and Kocaman, 2010; Turhan, 2017; Hernandez-Fontes et al., 2020). In the literature, image-processing techniques have been widely used for dam-break flow measurement (Liem and Kongeter, 1999; Aureli et al., 2011; Bechle and Wu, 2011; Yang et al., 2011; Kocaman and Ozmen-Cagatay, 2012; Turhan, 2017; Turhan

et al., 2019a,b). Numerous studies have considered the dam-break problem using both experimental and numerical methods (Ozmen-Cagatay and Kocaman, 2010; Minussi and Maciel, 2012; Oertel and Bung, 2012; Aureli et al., 2014; Turhan et al., 2019a,b; Wang et al., 2020). Dam-break flows for dry and wet bed conditions are typically treated separately due to the significant differences in the flow patterns (Stansby et al., 1998; Bukreev and Gusev, 2005; Khrabry et al., 2016; Lu et al., 2018; Hernandez-Fontes et al., 2020).

This current study focused on presenting new experimental data for dam-break waves over a dry bed in a rectangular and horizontal flume. The flow was numerically simulated by the industrial VOF- based CFD package, Flow-3D. A digital image processing technique was adopted for data acquisition from the laboratory experiments. Dam-break waves were generated by the sudden release of a movable gate, that divided the flume into a reservoir and downstream channel. In classical dam-break flow experiments, tap water has been used as fluid in the channel, whereas here, two more fluids of different densities: sunflower oil and salt water are also used in the experiment. To investigate the density and viscosity effects of Newtonian fluids on the dam-break flow, the sunflower oil was selected due to its low density and high viscosity compared to the water. To the authors' knowledge, sunflower oil has not previously been used before as a fluid in dam-break flow propagation. In published literature, there are isolated works concerning dam-break waves for different Newtonian and non-Newtonian fluids (Janosi et al., 2001; Ancy and Cochard, 2009; Li et al., 2013). In reality, the aim is to represent tailings dam, seawater, mud, debris and lava flows. This present study highlights the effects of various fluid densities on dam-break waves by obtaining instantaneous free-surface profiles at different times and flow depth variations over time, at specific locations. Using a small-scale laboratory setup was used to mirror the chaotic unsteady flow conditions during initial stages of the dam-break, since enclosed downstream channel end causes turbulence due to reflection of the flood wave from the end wall.

Investigating dam-break flow propagation is necessary for the development of emergency plans for flood hazards. In this study, experimental work and the numerical model of VOF- based RANS with the aid of Flow-3D are described in sections 2 and 3, respectively. In section 4, the numerical results are compared to the laboratory experiments. Finally, conclusions are summarized in section 5.

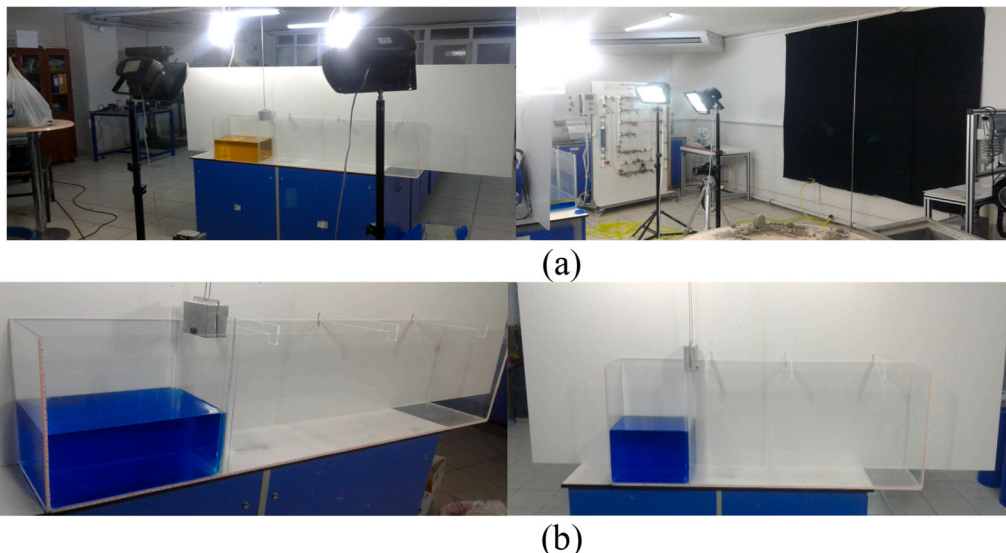
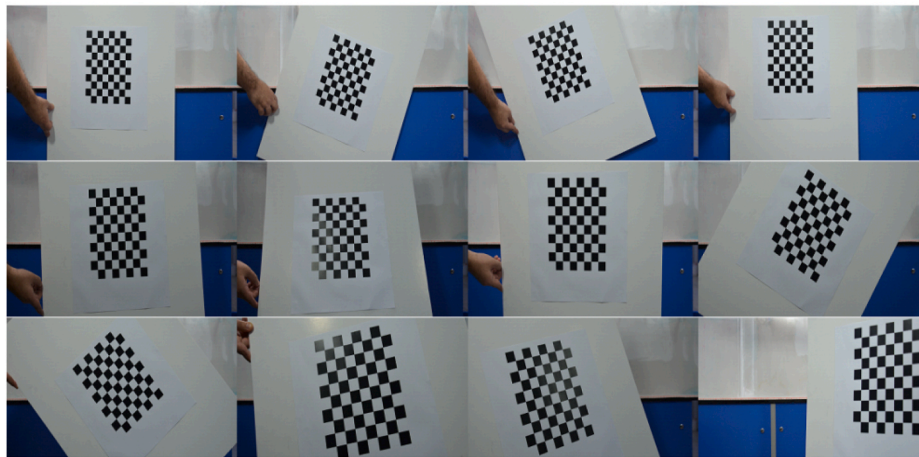


Fig. 2. Experimental set-up (a) Components of the set up (b) Gate mechanism.



(a)



(b)

Fig. 3. (a) Camera calibration settings, (b) Calibration board.

2. Experiment

2.1. Experimental set-up

The experimental set-up is at the laboratory of Adana Alparslan Turkes Science and Technology University, Turkey. The channel is rectangular and horizontal, with 1.216 m in length, 0.20 m in width and 0.32 m in height (see Fig. 1). The channel is made of with 5 mm thick plexiglas, except for the gate and clamps. The 3 mm-thick, 1 cm-wide plexiglas gate is placed at a distance of 0.30 m from the channel inlet in order to mirror a dam model. The gate fitted into channel-height

recesses created by four separate assemblies attached to the channel sides using chloroform acrylic glue. A 2 kg metal weight is attached by screws to the upper part of the gate acting as a fixed support between the gate and a pulley system. The weight prevents any leakage of the fluid from the reservoir to the downstream channel. The metal weight is attached by a rope and pulley system to a sandbag that lifted the weight up when the sandbag fell and released the fluid.

In addition, vaseline was applied to prevent leakage between the contact edges of the gate and the channel walls. In order to avoid the deformation of the channel, three plexiglas clamps were set up on the upper part of the channel at certain intervals. The experimental area was

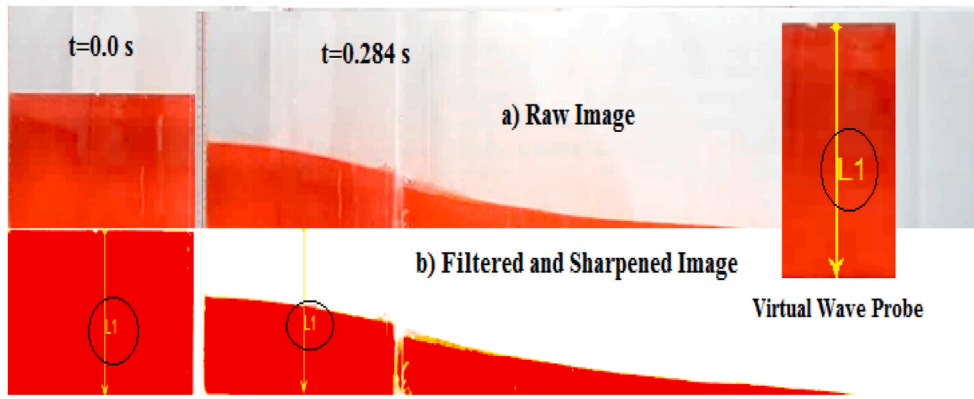


Fig. 4. The use of a virtual wave probe in time dependent salt water levels (a) raw image, (b) Filtered and sharpened image.

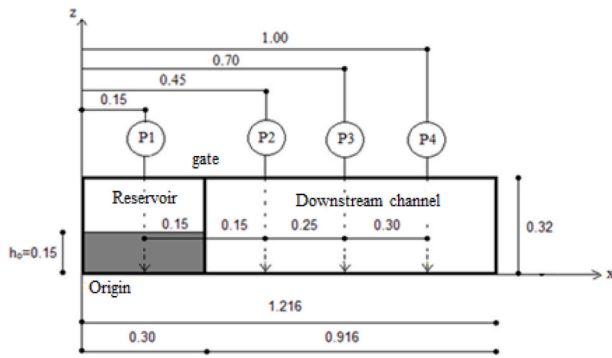


Fig. 5. Measurement locations with lengths in meters.

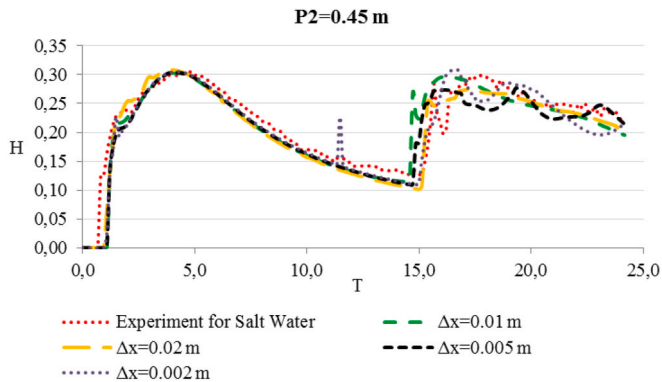


Fig. 6. Mesh sensitivity analysis at location P2 for salt water.

lit with constant light sources in order to avoid reflections and dark areas on the channel. Furthermore, a white styrofoam plate was put behind the channel to avoid reflections from any object in the test area. The complementary parts of the experimental set-up and the gate mechanism are presented in Fig. 2. In the experiments, the conditions for the sudden lifting of the gate were set. The upper limit of the sudden lifting time was determined to be $t = 0.155$ s for $h_0 = 0.15$ m according to the recommendation of the Lauber and Hager (1998) criterion that it should be shorter than $1.25 (h_0/g)^{1/2}$ for a “sudden removal” corresponding to 0.10 s in the present tests, from the video images. The Newtonian fluids in the reservoir were colored with various artificial food dyes to better observe the characteristics of the flow, except for sunflower oil with its natural yellow color.

Blue, yellow and red colors represent normal water, sunflower oil and salt water, respectively. One of the significant advantages of the

food coloring technique is allowing a homogeneous spread whilst not disturbing the flow. The density of the normal water is known to be 1000 kg/m^3 at a constant temperature of $T = 24 \text{ }^\circ\text{C}$ and that of sunflower oil is 910 kg/m^3 at $25 \text{ }^\circ\text{C}$. The density of the salt water was determined to be 1200 kg/m^3 for a 20% concentration value. The dynamic viscosity of the normal water was 0.001 kg/m.s at $T = 24 \text{ }^\circ\text{C}$. The dynamic viscosities of the sunflower oil and salt water were measured with the aid of a Brookfield viscometer at $24 \text{ }^\circ\text{C}$, to be 0.05 kg/m.s and 0.018 kg/m.s , respectively.

2.2. Flow measurement and camera calibration process

The calibration procedure was performed by pairing corner coordinates in diverse views of the calibration board (Fig. 3a). The distortions were calibrated using a calibration board containing black and white colored square meshes. The spatial calibration parameters were estimated by matching the known coordinates of the corners on video images that were recorded from 12 different viewpoints of the calibration board (Fig. 3b). Since the video images were taken with a camera in a fixed position, the error rate was very low. For the spatial calibration process, the GML Camera Calibration software program was used (Eaket et al., 2005; Ozmen-Cagatay and Kocaman, 2010; Bechle, and Wu, 2011; Evangelista et al., 2017; Ridolfi and Manciola, 2018). The images were captured by a camera with high resolution and high speed from the same locations. The basic characteristics of the camera are as follows: a full frame CMOS 24.7 megapixel image sensor; an effective pixel size of 24, 385,536; a native resolution of 24.4 megapixels; a Pro DSLR type lens montage, and an image format of FX/35 mm. Furthermore, the camera settings, such as the setting of the aperture, shutter speed and ISO, were adjusted according to the experimental conditions. The video images were captured at 1280×720 pixels and 60 frames per second (fps). Afterwards, the pixel data of the images were turned into lengths. Red stripes were fixed on the channel surface and the ground of the channel for analysis of the measurements. To identify the water-air interface better, resizing, filtering and contrast enhancement were applied to the raw images (Skoneczny, 2016). For details of these processes can be seen in Kocaman and Ozmen-Cagatay (2012). Thus the water-air interface was sharpened, and the exact location of the edge was accurately defined.

The depth changes of the Newtonian fluids over time at specified locations were measured directly from the video images without using any physical device, leaving the flow undisturbed. Thus, a procedure was applied with the aid of filter and edge recognition functions. In the process, numerous vertical lines can be drawn anywhere on the filtered and sharpened video images and they were considered to be virtual wave probes (Fig. 4) (Kocaman, 2007; Bechle and Wu, 2011; Kocaman and Ozmen-Cagatay, 2012; Campbel et al., 2014; Turhan et al., 2019a,b)

The measurement locations in the channel are listed as P1, P2, P3

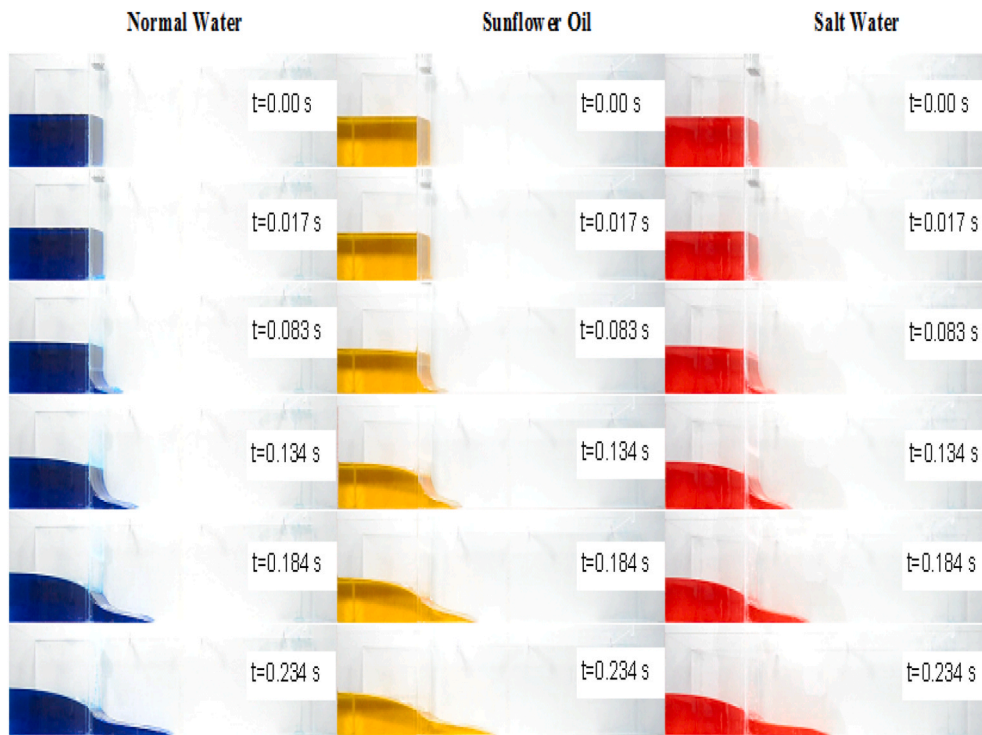


Fig. 7. Evolution of the free-surface profiles overtime at the initial stages, between $t = 0.00$ s to $t = 0.234$ s for the experiment.

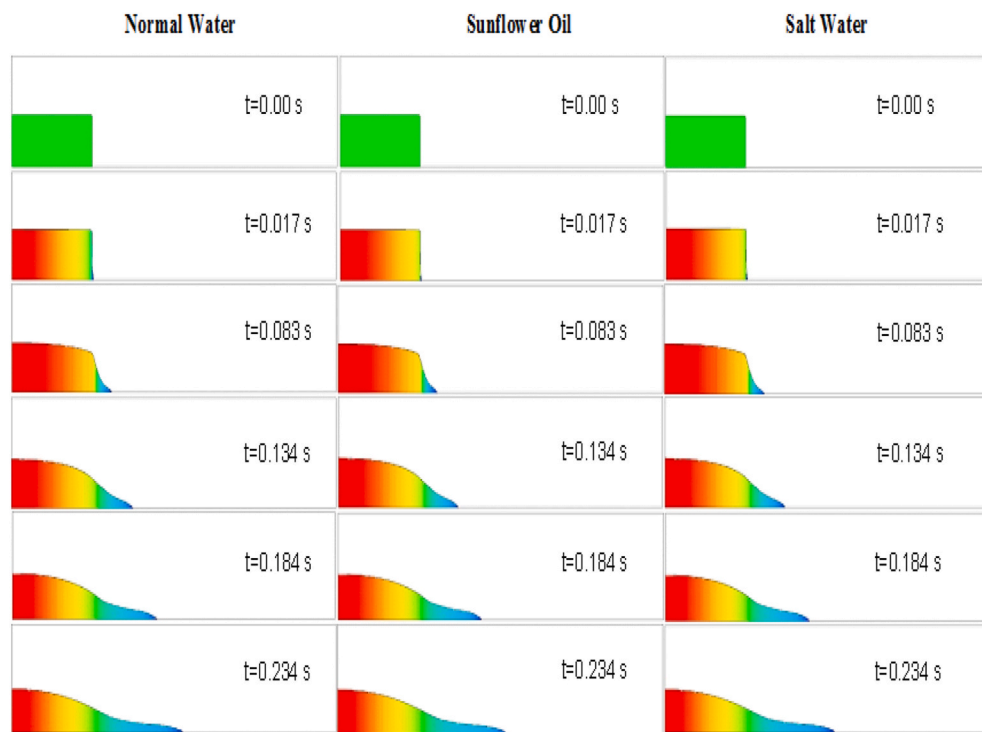


Fig. 8. Evolution of the free-surface profiles over time at the initial stages between $t = 0.00$ s to $t = 0.234$ s for RANS.

and P4 (Fig. 5). P1 was located at the midpoint of the reservoir and the others (P2, P3, and P4) were placed downstream. The level variations of the fluids over time were acquired in terms of that measurement location. Dimensionless magnitudes (H and T) were considered in this study and expressed as $H = h/h_0$ and $T = t (g/h_0)^{1/2}$ where, h , h_0 , g and t represent fluid height, initial reservoir height, gravitational acceleration and time, respectively.

3. Numerical modeling

3.1. Reynolds-averaged Navier–Stokes (RANS) Equations

The governing continuity (Equation (1)) and momentum (Equation 2) (RANS) equations for incompressible Newtonian fluid flow can be stated using Einstein's notation as follows (Wilcox, 2000;

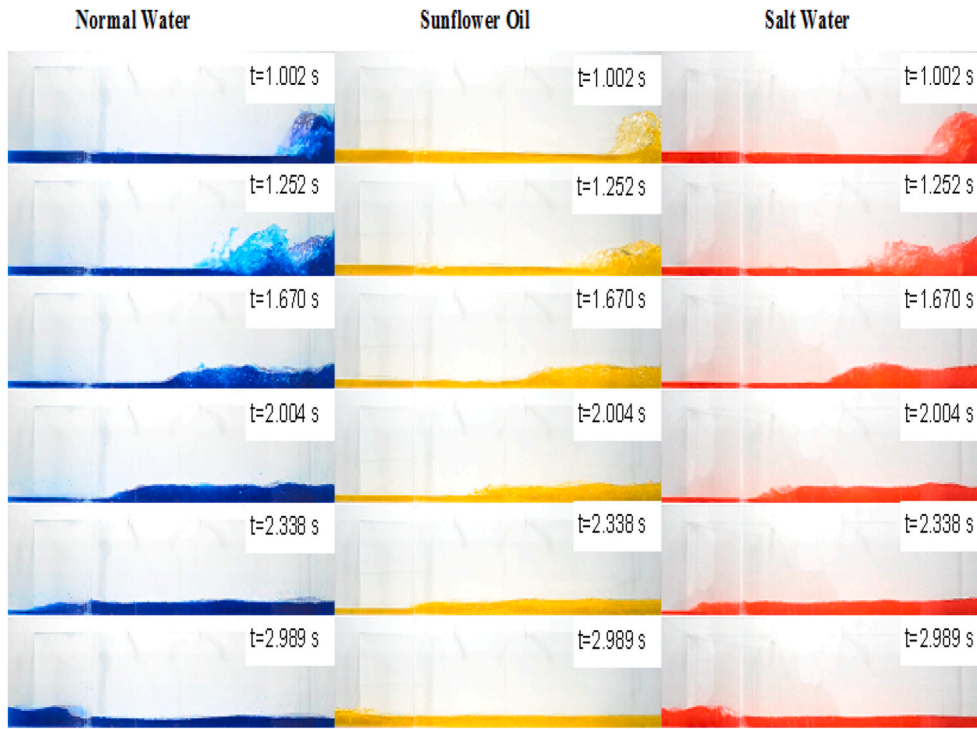


Fig. 9. Evolution of free-surface profiles of the reflected wave over time, from $t = 1.002$ s to $t = 2.989$ s for the experiment.

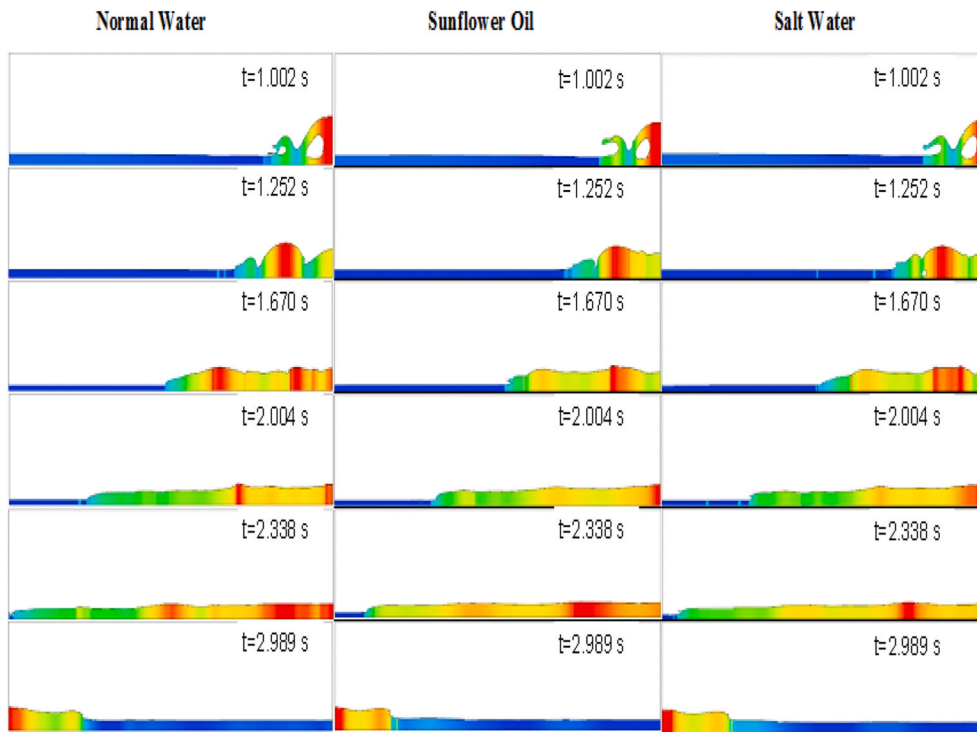


Fig. 10. Evolution of free-surface profiles of the reflected wave over time, from $t = 1.002$ s to $t = 2.989$ s for RANS.

Ozmen-Cagatay and Kocaman, 2010, 2011):

$$\frac{\partial}{\partial x_i} (u_i A_i) = 0 \quad (1)$$

$$\frac{\partial u_i}{\partial t} + \frac{1}{V_F} \left(u_j A_j \frac{\partial u_i}{\partial x_j} \right) = -\frac{1}{\rho} \frac{\partial p}{\partial x_i} + G_i + f_i \quad (2)$$

where x_i is the coordinate, u_i is the time-averaged velocity, A_j is the fractional area in a specified direction, t is the time, V_F is the fractional volume, p is the pressure, ρ is the density, G_i is the body accelerations and f_i is the viscous term defined by Equations (3) and (4):

$$f_i = \frac{1}{V_F} \left[\frac{\tau_{b,i}}{\rho} - \frac{\partial}{\partial x_j} (A_j S_{ij}) \right] \quad (3)$$

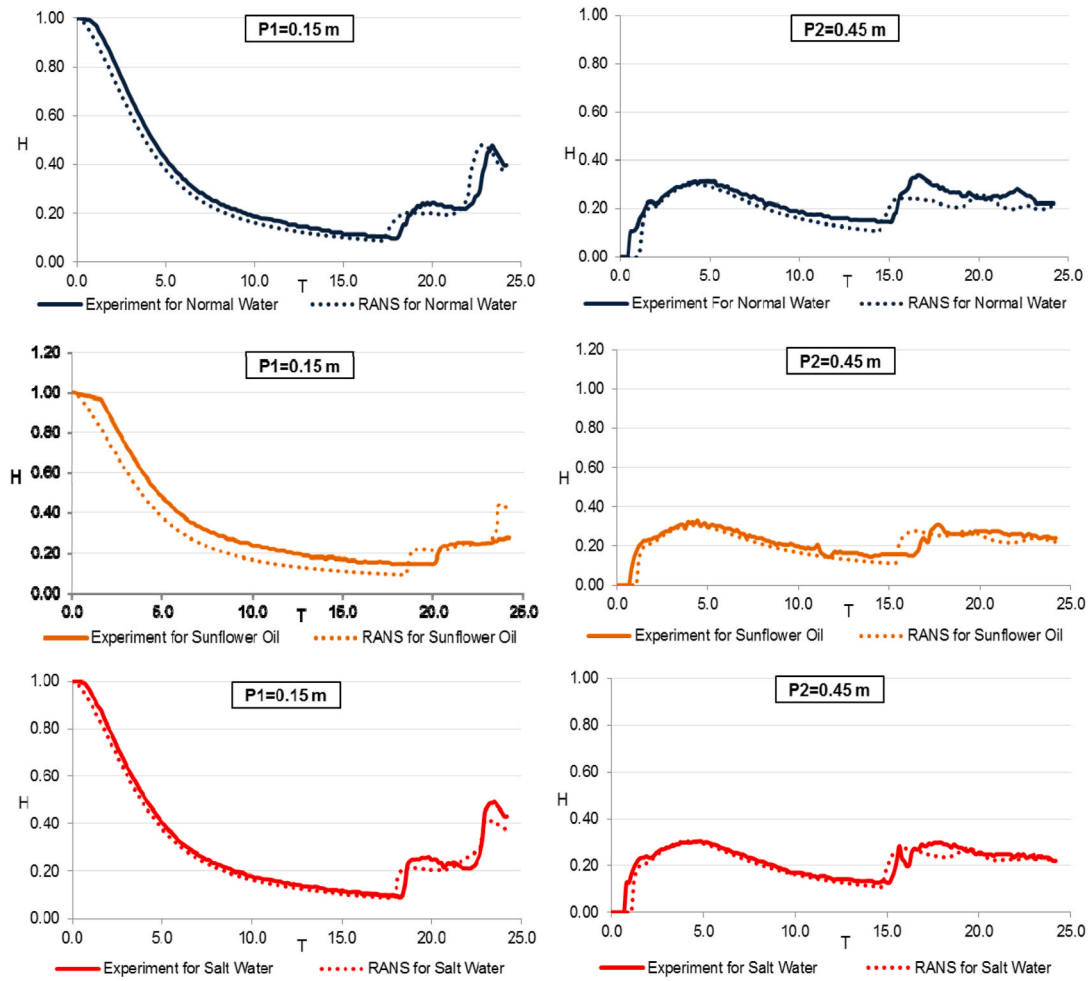


Fig. 11. Flow depth variations with time at P1 and P2.

$$S_{ij} = -(\nu + \nu_T) \left[\frac{\partial u_i}{\partial x_j} + \frac{\partial u_j}{\partial x_i} \right] \quad (4)$$

where $\tau_{b,i}$ represents wall shear stress, S_{ij} is the strain rate tensor, ν is the kinematic viscosity and ν_T is the kinematic eddy viscosity. The solution of the flow problems can be performed with the aid of different turbulence models (Wilcox, 2000; Ozmen-Cagatay et al., 2014; Yang et al., 2018). The $k-\epsilon$ turbulence model is possible method for the RANS simulations of dam-break flows (Shigematsu et al., 2004; Balabel, 2015; Kocaman and Ozmen-Cagatay, 2015; Turhan et al., 2019a,b). In this study, the $k-\epsilon$ turbulence model was applied for the numerical solution, given the former studies that used it to model rapidly varied unsteady flows at high Reynolds numbers (Lauder and Spalding, 1974; Kocaman and Ozmen-Cagatay, 2012; Flow Science, 2017; Turhan et al., 2018). In the $k-\epsilon$ turbulence model, turbulence eddy viscosity was calculated with the help of turbulence kinetic energy “ k ” and turbulent dissipation rate “ ϵ ” as follow in Equation (5):

$$\nu_T = \frac{C_\mu k^2}{\epsilon} \quad (5)$$

where C_μ is an empirical coefficient. In the standard model, the values of k and ϵ are specified from Equations (6a) and (6b):

$$\frac{\partial k}{\partial t} + u_i \frac{\partial k}{\partial x_i} = \frac{\partial}{\partial x_i} \left(\frac{\nu_t}{\sigma_k} \frac{\partial k}{\partial x_i} \right) + \nu_t \left(\frac{\partial u_i}{\partial x_j} + \frac{\partial u_j}{\partial x_i} \right) \frac{\partial u_i}{\partial x_j} - \epsilon. \quad (6a)$$

$$\frac{\partial \epsilon}{\partial t} + u_i \frac{\partial \epsilon}{\partial x_i} = \frac{\partial}{\partial x_i} \left(\frac{\nu_t}{\sigma_\epsilon} \frac{\partial \epsilon}{\partial x_i} \right) + C_{1\epsilon} \frac{\epsilon}{k} \nu_t \left(\frac{\partial u_i}{\partial x_j} + \frac{\partial u_j}{\partial x_i} \right) \frac{\partial u_i}{\partial x_j} - C_{2\epsilon} \frac{\epsilon^2}{k}. \quad (6b)$$

where the standard values of the empirical coefficients in the turbulence model are specified as $C_\mu = 0.09$, $C_{1\epsilon} = 1.44$, $C_{2\epsilon} = 1.92$, $\sigma_k = 1.0$ and $\sigma_\epsilon = 1.3$ (Balabel, 2015; Launder and Spalding, 1974). The numerical solutions for the RANS were calculated via the VOF- based CFD package, Flow-3D. This software program generates a mesh-grid system and includes a fractional area/volume obstacle representation method (FAVOR) using a cell porosity technique (Flow Science, 2017). All the surfaces of the channel are assumed smooth, which means the flow is accepted to be frictionless. Flow-3D allows the selections various surface roughness values according to the type of channel materials. In this simulation, the plexiglas channel roughness is ignored due to its very low value. The channel sidewalls were taken to be symmetrical, which implies no flux or shear of any feature across it. Tangential and normal velocities were assumed to be zero at the solid boundaries according to the no-slip condition (Kocaman and Ozmen-Cagatay, 2015; Turhan et al., 2019a,b). For this study, the grid size was taken to be 5 mm in both directions after carrying out sensitivity analysis. Mesh sensitivity was analyzed for four grid sizes of 2, 5, 10 and 20 mm (Fig. 6). Because of insignificant differences among the stage hydrographs, a grid size of 5 mm was adopted in this study. The time-step size is variable and automatically adjusted by respecting the Courant-Friedrichs-Lewy (CFL) stability criterion in Flow-3D. The numerical stability is ensured for $CFL < 1$ so that the fluid does not flow across more than one cell in one computational time step Δt . The CFL criterion is used in Flow-3D to

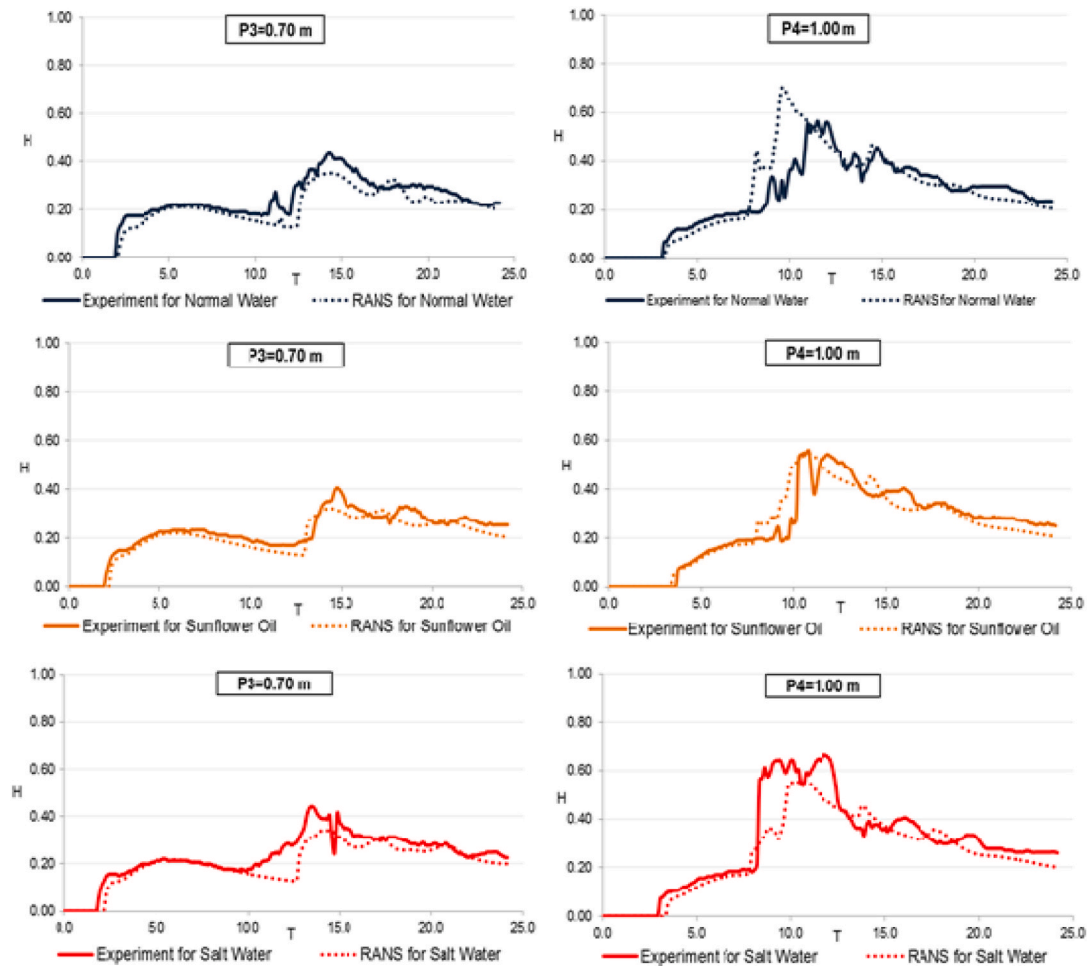


Fig. 12. Flow depth variations over time at P3 and P4.

calculate the maximum allowed time step size and it tells how fast the fluid passes through a cell. If the CFL is greater than 1, the velocity of a particle is so high that it passes through a cell in less than one time step. This leads to numerical instabilities. The minimum time step depends on its initial value and can be selected by the user. In this study, initial time step size Δt was taken to be 0.001 s. First-order momentum advection approximation was used in the RANS simulations, the implicit scheme was preferred to solve the equations in the numerical models. To track the free surface the VOF method was employed. The VOF method consists of three ingredients: a scheme to locate the surface, an algorithm to track the surface as a sharp interface moving through a computational grid, and a means of applying boundary conditions at the surface (Hirt and Nichols, 1981).

4. Results and discussion

In this study, dam-break induced wave propagations of three different Newtonian fluids were examined in a dry channel. Fig. 7 shows video images of the free-surface profiles, obtained from the experiment, which were digitized via image processing techniques. As the gate was abruptly lifted upwards, the fluid in the reservoir moved as an unsteady and turbulent downstream flow. Fig. 7 shows the evolution of the free-surface profiles over time, obtained from numerical RANS solution. The evolution over time of the free-surfaces was examined in two parts with respect to observed time periods. The first part points out the early initial stages from $t = 0.00$ s to $t = 0.284$ s (Figs. 7 and 8) and the other part, from $t = 1.002$ s to $t = 2.989$ s, indicated the reflection of the waves from the end wall (Fig. 9 and Fig. 10).

As can be seen in Fig. 7, at $t = 0.083$ s, the free-surface profiles are similar to the parabolic shape in all experiments. At the initial stages, there are similar results in the literature in case of dry bed conditions (Stansby et al., 1998; Bukreev and Gusev, 2005; Ozmen-Cagatay et al., 2014; Turhan et al., 2019a,b). After $t = 0.134$ s, free-surface profiles turned into convex shapes for all fluids. Hence, as time passes, the hydrostatic pressure becomes higher hydrostatic due to bottom friction, causing a convex free surface (Ozmen-Cagatay and Kocaman, 2010). According to Lauber and Hager (1998), a dam-break wave over a dry bed can be divided into an initial wave and a dynamic wave passing the initial stage at a defined section. This event was observed over the dry bed in numerous previous works (Stansby et al., 1998; Aureli et al., 2011; Oertel and Bung, 2012; Lu et al., 2018; Turhan et al., 2019a,b). Figs. 9 and 10 show the free-surface profiles for a reflected wave from the end wall over time for the experimental and numerical model, respectively.

At $t = 1.002$ s, the wave rises on the channel surface and air bubbles emerge on the front of the wave. High energy losses in the experiments caused a decrease in the velocity on account of the turbulence effects and the levels of all the fluids were higher than those of the numerical results (Ozmen-Cagatay and Kocaman, 2010; Turhan et al., 2018, 2019). At $t = 1.252$ s, shapes of the wave fronts for all fluids were different from each other. In the case of the oil, a small wave break was observed, whereas a significant wave break occurred in the other fluids. It indicated that the wave front velocity of the oil was lower than the other fluids due to the viscosity effect. It can be seen from Figs. 9 and 10 that there is good agreement between experimental data and RANS outcomes. In the published literature, the RANS solution produces good

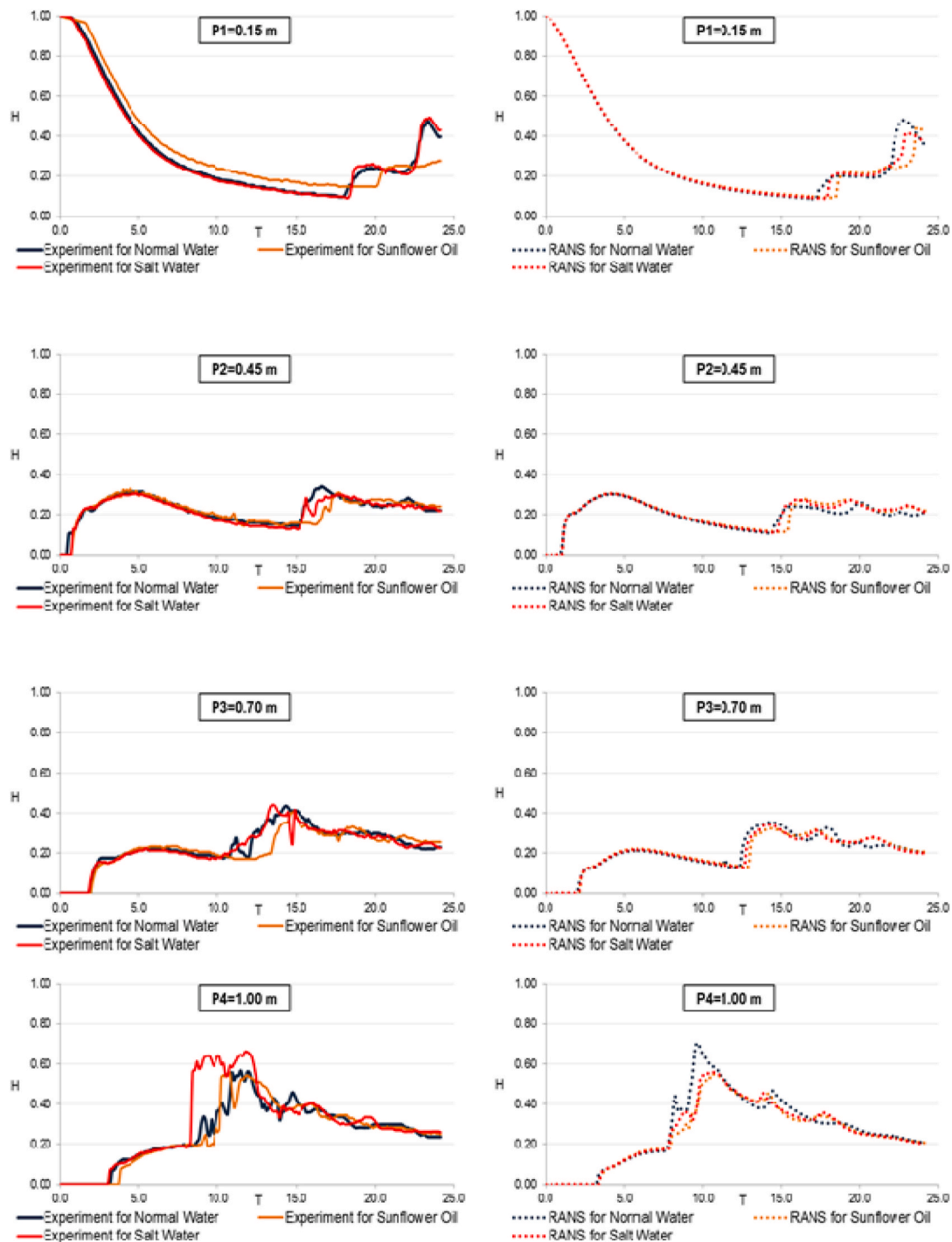


Fig. 13. Measured and computed comparison of the flow depth variations over time for three fluids at P1, P2, P3, and P4.

results in dam-break flow investigation (Shigematsu et al., 2004; Ozmen-Cagatay and Kocaman, 2010; Ozmen-Cagatay et al., 2014; Marsooli and Wu, 2014; Kamra et al., 2018; Yang et al., 2018). As seen from Fig. 11, for normal and salt water at P1 (0.15 m), although the levels of the flows in experiment are slightly higher than those of the numerical results, there was reasonable agreement between the experimental data and numerical results. As for sunflower oil at P1, the difference between experimental data and numerical result increased. At P2 (0.45 m), RANS solution produced good results for sunflower oil and salt water, however, it underestimated the flow depths after $T = 16$ for normal water.

As can be seen from Fig. 12, at P3 (0.70 m), the experimental results

obtained were higher than the numerical results. The differences in the graphs were high between $T = 10$ and 20 . At P4 (1.00 m), some fluctuations can be seen in the graphs of the experimental results for all three cases. While the best agreement of numerical results with experimental results were observed for sunflower oil, the most deviations between experimental and RANS simulation at P4 for normal water. Here, the numerical solution overestimated the flow depth from $T = 8$ to $T = 12$ for normal water. Finally, predictions using RANS generally display good agreement with the measurement except for the time interval from $T = 8$ to $T = 12$.

Fig. 13 compares the measured and numerically computed flow depth variations over time for three fluids at four locations: P1, P2, P3,

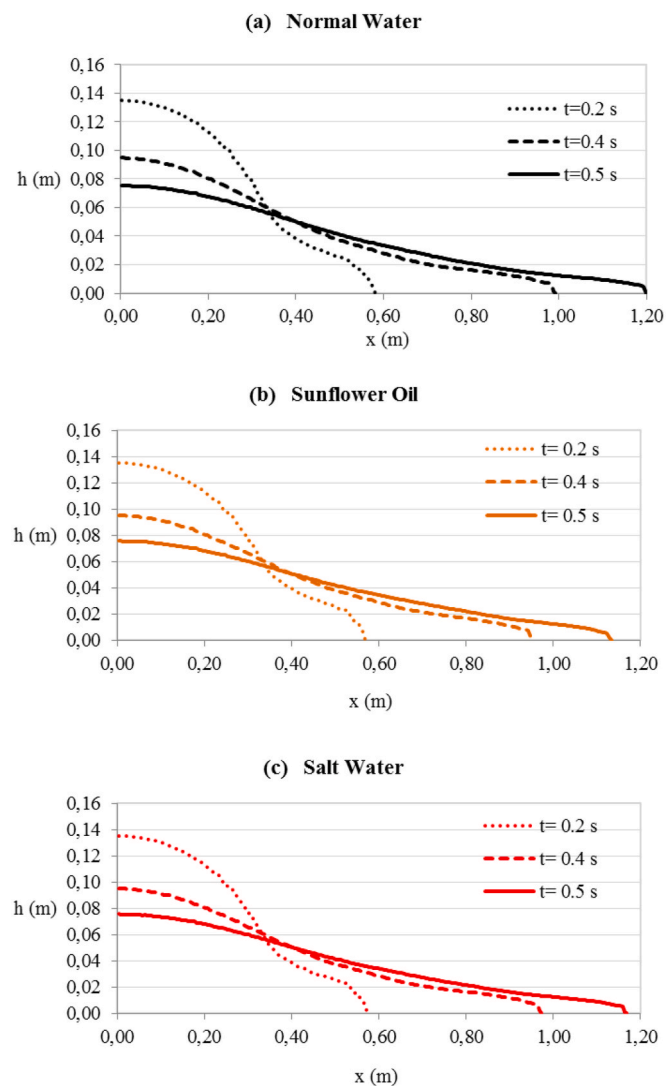


Fig. 14. Evolution of the numerically computed wave fronts at the initial stages, (a) for normal water (b) for sunflower oil (c) for salt water.

and P4. While the three results were close to each other at P1 in the RANS solution except for the time interval from $T = 23$ to $T = 25$, in the measured results, sunflower oil depth was higher than those of other fluids up to $T = 18$ and it was lower than others after $T = 18$. Despite disagreement at P2 in the vicinity of the second peak ($T = 15$ to $T = 17$) in the experiment, general agreement was good between all fluids. In RANS solution at location P2, the three results were close to each other except for the time interval from $T = 23$ to $T = 25$. As shown in Fig. 13, fluctuations were observed at P3 from $T = 11$ to $T = 16$ in the experimental results due to turbulence effect and the level of sunflower oil is lower than those of other fluids, however, RANS solution cannot predict the fluctuations. At P4, discrepancies between the measured and computed results are shown in the graphs. The measured result for salt water was different from the others from $T = 8$ to $T = 12$. While the depth of salt water was higher than the other fluids in the measured results, the normal water depth was higher in the computed results at P4. During the initial stages of dam-break flow, the propagations of three Newtonian fluids with different densities displayed similar behavior at almost all locations except P4 (Fig. 13). However, a few discrepancies occurred with the progression of time, especially in the experimental results.

Fig. 14 shows evolution of the numerically computed wave fronts at the initial stages for normal water, sunflower oil and salt water. The

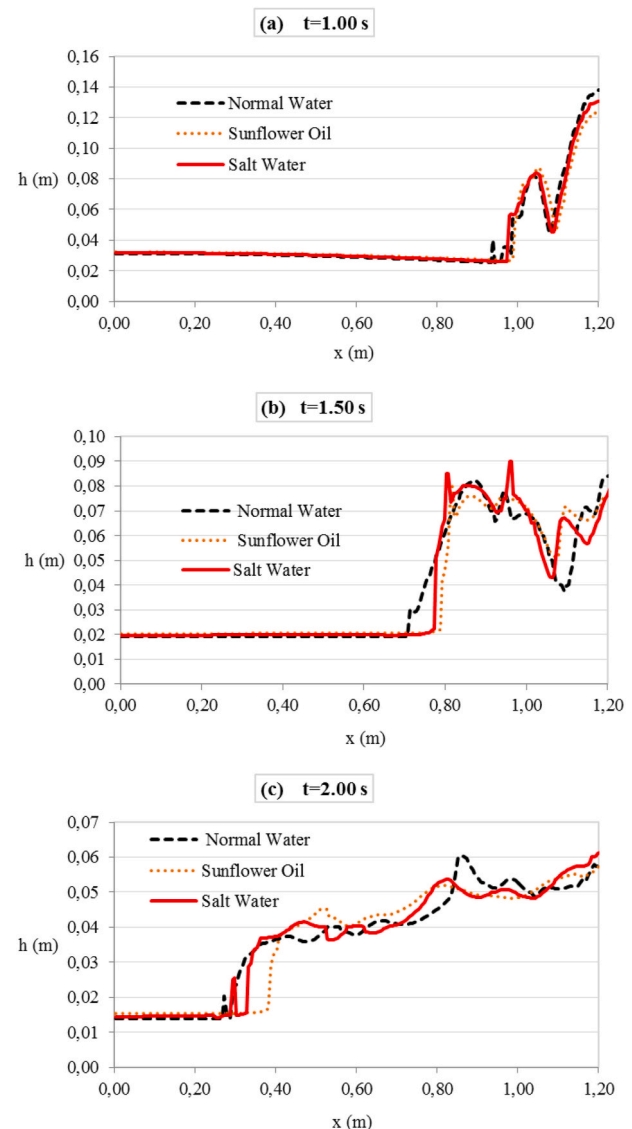


Fig. 15. Evolution of the numerically computed rarefaction waves (a) $t = 1$ s. (b) $t = 1.5$ s. (c) $t = 2,0$ s.

density and viscosity effects can be slightly seen on the graphs.

Fig. 15 shows evolution of the numerically computed rarefaction wave in the upstream direction. Although there are almost no differences among three graphs of fluids at $t = 1$ s, the differences in celerity of the negative wave fronts for three fluids can be clearly distinguished at $t = 1.5$ s and $t = 2$ s. The density and viscosity effects of the salt water and sunflower oil are obviously seen.

5. Conclusion

This study considered the propagation of flood waves resulting from dam-breaks in an initially dry channel for various Newtonian fluids with different densities (normal water, sunflower oil and salt water). New experiments were conducted in a rectangular channel with a smooth horizontal dry bed. Snapshots were obtained with a digital image technique of the instantaneous free-surface profiles at different times, and of the flow–depth hydrographs at certain locations. A small-scale laboratory setup was used that mirrored the chaotic flow conditions, since the enclosed downstream channel end caused turbulence due to the flood wave reflection from the end wall during the initial stages of the dam break. At these initial stages, the results obtained from the

experiments with all three fluids showed similar behavior with each other'. As the flow progressed, discrepancies occurred because of turbulence and frictional effects. Thus, the free-surface profiles of the wave front changed over time and wave front velocity was different for each fluid. While the propagation for all fluids was similar at the initial stages of motion, the effect of the end channel wall induced differences in depths and wave front velocities, particularly, for the sunflower oil moving slowly due to its high viscosity. The VOF-based RANS model program Flow-3D was used to generate numerical results to compare with the experiments. The numerical simulation results showed good overall agreement with the experimental data. Although the numerical model has difficulty in estimating turbulence and friction effects, its prediction of the flow can be reasonably acceptable. Comparison of the numerical results with the experimental data revealed the abilities and shortcomings of the numerical model. As a result, the laboratory data presented in this work may be useful in the validation of other numerical studies. In the future, force and velocity measurements for the dam-break flow problems for several fluids and the effects of various channel base conditions on flow characteristics can be investigated in detail.

CRedit authorship contribution statement

Hatice Ozmen-Cagatay: wrote the manuscript. **Evren Turhan:** carried out the experiments. **Selahattin Kocaman:** performed the numerical simulation.

Declaration of competing interest

None' in the template.

Acknowledgements

This study was supported by Cukurova University Research Fund Project No. FDK-2015-4887. The authors gratefully acknowledge this support.

References

- Ancey, C., Cochard, S., 2009. The dam-break problem forerschel-Bulkley viscoplastic fluids down steep flumes. *J. Non-Newtonian Fluid Mech.* 158, 18–35.
- Aureli, F., Maranzoni, A., Mignosa, P., Ziveri, C., 2011. An image processing technique for measuring free surface of dam break flows. *Exp. Fluid* 50, 665–675.
- Aureli, F., Dazzi, S., Maranzoni, A., Mignosa, P., Vacondio, R., 2014. Experimental and numerical evaluation of the force due to the impact of a dam-break wave on a structure. *Adv. Water Resour.* 76, 29–42.
- Balabel, A., 2015. Numerical simulation of turbulent dam-break flow using the level set method. *Int. J. Mod. Phys. 1* (3), 112–117.
- Balcazar, N., Lehmkuhl, O., Jofre, L., Rigola, J., Oliva, A., 2016. A coupled volume-of-fluid/level-set method for simulation of two-phase flows on unstructured meshes. *Comput. Fluid* 124 (2), 12–29.
- Bechle, A.J., Wu, C.H., 2011. Virtual wave gauges based upon stereo imaging for measuring surface wave characteristics. *Coast. Eng.* 58 (4), 305–316.
- Bellos, V., Soulis, J.V., Sakkas, J.CampbelG., 1992. Experimental investigation of two-dimensional dam-break induced flows. *J. Hydraul. Res.* 30 (1), 47–63.
- Biscarini, C., Francesco, S. Di, Manciola, P., 2010. CFD modeling approach for dam break flow studies. *Hydrol. Earth Syst. Sci.* 14, 705–718.
- Bukreev, V.I., Gusev, A., 2005. Initial stage of the generation of dam-break waves. *Dokl. Phys.* 50 (4), 200–203.
- Campbell, A.J., Bechle, A.J., Wu, C.H., 2014. Observations of surface waves interacting with ice using stereo imaging. *J. Geophys. Res.: Oceans* 119, 3266–3284.
- Cantero-Chinchilla, F.N., Castro-Orgaz, O., Khan, A.A., 2019. Vertically-averaged and moment equations for flow and sediment transport. *Adv. Water Resour.* 132, 103387.
- Chanson, H., Aoki, S., Maruyama, M., 2003. An experimental study of tsunami runup on dry and wet horizontal coastlines. *Sci. Tsunami Hazards* 20, 278–293.
- Eaket, J., Hicks, F.E., Peterson, A.E., 2005. Use of stereoscopy for dam break flow measurement. *J. Hydraul. Eng.- ASCE* 131 (1), 24–29.
- Evangelista, S., Giovenco, G., Kocaman, S., 2017. A multi-parameter calibration method for the numerical simulation of morphodynamic problems. *J. Hydrol. Hydromechanics* 65 (2), 175–182.
- Flow Science Inc, 2017. Flow-3D User Manual. Flow Science, Santa Fe, NM.
- Gu, Z.H., Wen, H.L., Yu, C.H., Sheu, T.W.H., 2018. Interface-preserving level set method for simulating dam-break flows. *J. Comput. Phys.* 374, 249–280.
- Hernandez-Fontes, J.V., Vitola, M.A., Esperanca, P.T.T., et al., 2020. Patterns and vertical loads in water shipping in systematic wet dam-break experiments. *Ocean Eng* 197, 106891.
- Hirt, C.W., Nichols, B.D., 1981. Volume of fluid method for the dynamics of free boundaries. *J. Comput. Phys.* 39 (1), 201–225.
- Hu, H., Zhang, J., Li, T., 2018. Dam-break flows: comparison between Flow-3D, MIKE 3 FM, and analytical solutions with experimental data. *MDPI Appl. Sci.* 8 (12), 2456–2480.
- Issakhov, A., Imanberdiyeva, M., 2019. Numerical simulation of the movement of water surface of dam break flow by VOF methods for various obstacles. *Int. J. Heat Mass Tran.* 136, 1030–1051.
- Issakhov, A., Borsikbayeva, A., 2021. Numerical simulation of the water surface movement with macroscopic particles on movable beds for inhomogeneous relief. *J. Hydraul. Res.* <https://doi.org/10.1080/00221686.2020.1869603>.
- Janosi, I.M., Jan, D., Szabo, K.G., Tel, T., 2001. Turbulent drag reduction in dam-break flows. *Exp. Fluid* 37, 219–229.
- Kamra, M.M., Mohd, N., Liu, C., Sueyoshi, M., Hu, C., 2018. Numerical and experimental investigation of three-dimensionality in the dam-break flow against a vertical wall. *J. Hydrodyn.* 30 (4), 682–693.
- Kesserwani, G., Shaw, J., Sharifian, M.K., et al., 2019. (Multi)wavelets increase both accuracy and efficiency of standard Godunov-type hydrodynamic models. *Adv. Water Resour.* 129, 31–55.
- Khoshkonesh, A., Nsom, B., Gohari, S., Banejad, H.A., 2019. Comprehensive study on dam-break flow over dry and wet beds. *Ocean Eng* 188, 106279.
- Khrabry, A., Smirnov, E., Zaytsev, D., Goryachev, V., 2016. Numerical study of 2D and 3D separation phenomena in the dam-break flow interacting with a triangular obstacle. *Period. Polytech. - Mech. Eng.* 60 (3), 159–166.
- Kocaman, S., 2007. Experimental and Theoretical Investigation of Dam-Break Problem. Ph. D. Thesis. Civ. Engng. Dept., University of Cukurova, Adana, Turkey [in Turkish].
- Kocaman, S., Ozmen-Cagatay, H., 2012. The effect of lateral channel contraction on dam break flows: laboratory experiment. *J. Hydrol* 432–433, 145–153.
- Kocaman, S., Ozmen-Cagatay, H., 2015. Investigation of dam-break induced shock waves impact on a vertical wall. *J. Hydrol.* 525, 1–12.
- Lauber, G., Hager, W.H., 1998. Experiments to dam break wave: horizontal channel. *J. Hydraul. Res.* 36 (3), 291–308.
- Lauder, B.E., Spalding, D.B., 1974. The numerical computation of turbulent flows. *Comput. Methods Appl. Math.* 3 (2), 269–275.
- Li, Y.L., Yu, C.H., 2019. Research on dam-break flow induced front wave impacting a vertical wall based on the CLSVOF and level set methods. *Ocean Eng* 178, 442–462.
- Li, G., Oka, Y., Furuya, M., Kondo, M., 2013. Experiments and MPS analysis of stratification behavior of two immiscible fluids. *Nucl. Eng. Des.* 265, 210–221.
- Liem, R., Kongeter, J., 1999. Application of High-Speed Digital Image Processing to Experiments on Dam Break Waves. Proc. CADAM Meeting, Zaragoza, pp. 399–411. Spain.
- Lu, S., Liu, H., Deng, X., 2018. An experimental study of the run-up process of breaking bores generated by dam-break under dry- and wet-bed conditions. *J. Earthq. Tsunami* 12 (2), 1840005–1840012.
- Marsooli, R., Wu, W., 2014. 3-D finite-volume model of dam-break flow over uneven beds based on VOF method. *Adv. Water Resour.* 70, 104–117.
- Minussi, R.B., Maciel, G.D.F., 2012. Numerical experimental comparison of dam break flows with non-Newtonian fluids. *J. Braz. Soc. Mech. Sci. Eng.* 34 (2), 167–178.
- Ningegowda, B.M., Premachandran, B., 2014. A Coupled Level Set and Volume of Fluid method with multi-directional advection algorithms for two-phase flows with and without phase change. *Int. J. Heat Mass Tran.* 79, 532–550.
- Oertel, M., Bung, D.B., 2012. Initial stage of two-dimensional dam-break waves laboratory versus VOF. *J. Hydraul. Res.* 50 (1), 89–97.
- Ozgozmen, T.M., Iliescu, T., Fischer, P.F., Srinivasan, Duan, J., 2007. Large eddy simulation of stratified mixing in two-dimensional dam-break problem in a rectangular enclosed domain. *Ocean Sci.* 16 (1–2), 106–140.
- Ozmen-Cagatay, H., Kocaman, S., 2010. Dam-break flows during initial stage using SWE and RANS approaches. *J. Hydraul. Res.* 48 (5), 603–611.
- Ozmen-Cagatay, H., Kocaman, S., 2011. Dam-break flow in the presence of obstacle: experiment and CFD simulation. *Eng. Appl. Comp. Fluid Mech.* 5 (4), 541–552.
- Ozmen-Cagatay, H., Kocaman, S., Guzel, H., 2014. Investigation of dam-break flow waves in a dry channel with a hump. *J. Hydro-Environ. Res.* 8, 304–315.
- Prabu, P., Bhallamudi, S.M., Chaudhuri, A., Sannasiraj, S.A., 2019. Numerical investigations for mitigation of tsunami wave impact on onshore buildings using sea dikes. *Ocean Eng* 187, 106159.
- Ridolfi, Manciola, 2018. Water level measurements from drones: A pilot case study at a dam site. *Water* 10 (3), 297. <https://doi.org/10.3390/w10030297>.
- Ritter, A., 1892. Die fortpflanzung der Wasserwellen. *Zeitschrift Verein Deutscher Ingenieure* 36 (33), 947–954 (in German).
- Shigematsu, T., Liu, P.L.F., Oda, K., 2004. Numerical modeling of the initial stages of dam-break waves. *J. Hydraul. Res.* 42 (2), 183–195.
- Skoneczny, S., 2016. Morphological sharpening of color images. *Bull. Pol. Acad. Sci. Tech. Sci.* 64 (1), 103–113.
- Soleimani, K., Ketabdari, M.J., 2020. Meshfree modeling of near field two-liquid mixing process in the presence of different obstacles. *Ocean Eng* 213, 107625.
- Stansby, P.K., Chegini, A., Barnes, T.C.D., 1998. The initial stages of dam-break flow. *J. Fluid Mech.* 374, 407–424.
- Stoker, J.J., 1957. *Water Waves*. Interscience Publishers, Wiley, New York, pp. 333–341.
- Tayfur, G., Guney, M.S., 2013. A physical model to study dam failure flood propagation. *Water Utility Journal* 6, 19–27.

- Turhan, E., 2017. The Investigation of Dam-Break Flow Using with Experimental and Smoothing Particle Hydrodynamics (SPH) Methods. Cukurova University, Institute of Natural and Applied Sciences, Adana. PhD Thesis.
- Turhan, E., Dal, K., Ozmen-Cagatay, H., Kocaman, S., 2018. An Experimental and Numerical Study of Dam-Break Flow Problem with Different Density Fluid. 5th International Dam Safety Symposium, pp. 1426–1437. Istanbul.
- Turhan, E., Ozmen-Cagatay, H., Kocaman, S., 2019a. Experimental and numerical investigation of shock wave propagation due to dam-break over wet channel. *Pol. J. Environ. Stud.* 28 (6), 1–24.
- Turhan, E., Ozmen-Cagatay, H., Tantekin, A., 2019b. Modeling flood shock wave propagation with the smoothed particle hydrodynamics (SPH) method: an experimental comparison study. *Appl. Ecol. Environ. Res.* 17 (2), 3033–3047.
- Wang, B., Liu, W., Wang, W., et al., 2020. Experimental and numerical investigations of similarity for dam-break flows on wet bed. *J. Hydrol.* 583, 124598.
- Wilcox, D.C., 2000. Turbulence Modeling for CFD. DCW Industries, Inc., La Canada, CA.
- Yang, X., Wei-lin, X., Shu-jing, L., Hua-yong, C., Nai-wen, L., 2011. Experimental study of dam-break flow in cascade reservoirs with steep bottom slope. *J. Hydrodyn.* 23 (4), 491–497.
- Yang, S., Yang, W., Qin, S., et al., 2018. Numerical study on characteristics of dam-break wave. *Ocean Eng* 159, 358–371.
- Yang, S., Yang, W., Qin, S., Li, Q., 2019. Comparative study on calculation methods of dam-break wave. *J. Hydraul. Res.* 57 (5), 702–714.
- Yu, C.H., Wen, H.L., Gu, Z.H., An, R.D., 2019. Numerical simulation of dam-break flow impacting a stationary obstacle by a CLSVOF/IB method. *Commun. Nonlinear Sci. Numer. Simulat.* 79, 104934.
- Zhang, S., Tan, Y., 2014. Risk assessment of earth dam overtopping and its application research. *Nat. Hazards* 74 (2), 717.